J. Fluid Mech. (1976), *vol.* 73, *part* 3, *pp.* 427–444
Printed in Great Britain

Long-wave decay due to convective turbulence

By THEODORE GREEN AND SEE WHAN KANG
Marine Studies Center, The University of Wisconsin, Madison

(Received 1 July 1974 and in revised form 10 March 1975)

Long waves are generated in a laboratory-size rectangular basin, which is heated uniformly from below. Their subsequent decay is measured, and the decay component due to the action of convective turbulence isolated, using a combination of existing theories and interpretation techniques. An expression is proposed for the turbulent decay decrement as a function of the bulk Rayleigh number. The results agree as well as can be expected with a simple model based on a Reynolds-stress decay estimate obtained by superposing convective thermals on the oscillating flow associated with the long wave.

1. Introduction

Long waves play a rather important role in geophysical fluid mechanics. Because of this, considerable attention has been devoted to the generation of long water waves by wind stress and atmospheric pressure variations. Somewhat less attention has been paid to long-wave decay, although the persistence (thus, death) of any phenomenon would seem almost equally important as its growth. None the less, the general nature of many of the mechanisms involved in the decay of long waves is clear. Bottom friction is normally the primary cause of decay, and has been parameterized in several numerical models. Absorbing barriers and wave breaking play an important role in harbours and along open coasts. Opposing winds and atmospheric pressure patterns can also lead to wave decay. Compared with these factors, the effect of internal friction is almost always negligible.

Additional factors must be considered in laboratory-scale situations. Wall friction is usually significant. Free-surface effects can also lead to substantial energy loss: surface films may increase viscous dissipation noticeably; capillary hysteresis due to changing contact angles associated with the vertical motion of the fluid at the container walls can be important. The number of detailed experimental studies of wave decay is still small, however, and some of the basic decay mechanisms are not yet sufficiently well understood to permit confident parameterization. This paper deals with one such mechanism: turbulence.

Turbulence can cause wave decay through two processes (Phillips 1959). The organized wave energy can be scattered effectively when the scale of the energy-containing eddies is similar to that of the waves. If the turbulence scale is much smaller than the wave scale, wave energy is lost through an eddy-viscosity mechanism. Little experimental work has been directed at either process. That

which has (e.g. Green, Medwin & Paquin 1972) concerns the interaction of short surface waves with some type of grid turbulence.

A common cause of geophysical turbulence is gravitational instability. In water bodies, this is usually due to prolonged surface cooling. Although not completely understood, this convective turbulence has been studied relatively thoroughly in the laboratory (e.g. Townsend 1959; Deardorff & Willis 1967), and semi-empirical theories have been quite successful in describing some of its properties (Howard 1967). The experiment described below constitutes a first step in understanding the interaction between long waves and convective turbulence.

2. Long-wave decay due to convective turbulence

The intensity of convective turbulence is closely related to the static instability of a layer of fluid. The bulk Rayleigh number $Ra = \beta g h^3 \Delta T / \kappa \nu$ is a good measure of the associated kinetic energy. Here, β is the coefficient of thermal expansion, g gravity, h layer depth, ν kinematic viscosity, κ thermometric conductivity, and ΔT the absolute (unstable) temperature difference over the layer. The quantities κ and ν are evaluated at the mean fluid temperature. Malkus (1954) determined the turbulent kinetic energy density to be an increasing function of Ra, beginning at $Ra \sim 10^3$, where the fluid layer first becomes dynamically unstable. Geophysical Rayleigh numbers can be quite large. When the convective kinetic energy is comparable with the long-wave energy in the layer, one may expect the wave motion to be measurably affected.

Sparrow, Husar & Goldstein (1970), Townsend (1959) and others showed high-Ra turbulent convection to consist of an almost periodic series of bursts of fluid from the lower laminar boundary layer (say) into the uniformly turbulent fluid above. These thermals occur over only a small fraction of the bottom boundary, and are quite stable in position. When the thermals are coupled with the horizontal oscillatory motion associated with a long wave, a net vertical transfer of horizontal momentum leads to an effective bottom shear stress, and hence to decay of the wave. At least for long waves, this absorption mechanism seems simpler to understand than scattering, which depends crucially on turbulent vorticity fluctuations.

There are, of course, fundamental questions that are ignored in this simple explanation. For example, it is unclear how the conduction layer of thickness $\Delta \sim 3(\rho c T_0 \kappa^3 / g Q)^{\frac{1}{4}}$ interacts with the oscillatory boundary layer of thickness $\delta \sim (\nu/\sigma)^{\frac{1}{2}}$ associated with the long wave. Here, Q is upward heat flux, T_0 the absolute bottom temperature, c specific heat, ρ density, and σ wave frequency. It is also unclear at what point the oscillatory shear flow will significantly change the burst type of convective turbulence described above. Although these and other details are crucial to a full understanding of the phenomenon, we shall ignore them, and concentrate on the resulting wave decay, a more easily measured integral property of the flow. Future work will be directed towards eliciting more fundamental aspects of the interaction between long waves and convective turbulence.

A very simple model, which allows an order-of-magnitude estimate of the Reynolds stress $\tau = -\overline{\rho u' w'}$ near the bottom, can easily be developed. Here, the bar denotes an average across the tank. The vertical turbulent velocity component w' is due mainly to the thermals, with scale velocity W. The horizontal component u' stems from the rapid change in fluid velocity over the oscillatory bottom boundary layer. Then the Reynolds stress can be written $\tau = n\rho UW$, where U is the horizontal velocity component associated with the long wave, and n is a small, unknown number reflecting the fraction of horizontal area over which thermals occur and, to some extent, the actual correlation between u' and w' near the bottom.

The linearized one-dimensional long-wave equations of motion are

$$\frac{\partial U}{\partial t} + \frac{nW}{h} U + g\frac{\partial \eta}{\partial x} = 0, \quad h\frac{\partial U}{\partial x} + \frac{\partial \eta}{\partial t} = 0. \tag{1}$$

(η is surface height above mean water level, x horizontal distance, and t time.) Here, τ has been treated as a body force in the usual manner and other contributions to decay have been neglected. The fundamental-mode solution for free oscillations of initial amplitude a_0 in a rectangular basin of length L is closely

$$\eta = a_0(x) \exp\left[-nWt/(2h)\right] \cos (gh)^{\frac{1}{2}} kt. \tag{2}$$

(The wavenumber $k = \pi/L$.) We define the turbulent logarithmic decay decrement α_T by writing the amplitude function as $a_0(x) \exp(-\alpha_T t/T)$, where T is the wave period $2L/(gh)^{\frac{1}{2}}$. Then

$$\alpha_T = nWL/(gh^3)^{\frac{1}{2}}. \tag{3}$$

This simple estimate for α_T applies only where the oscillatory long-wave motion does not substantially alter the burst-type of convective turbulence discussed above. With this proviso, both the mechanism and the decay estimate are independent of the wave-turbulence kinetic energy ratio.

In what follows, we describe an experiment leading to an independent estimate of α_T.

3. Previous work

Probably the simplest way to study wave decay experimentally is to measure standing-wave dissipation in a cylindrical container in the laboratory. We used this technique. Three other studies are most germane to our work; only the pertinent results are recounted here.

Keulegan (1959) studied fundamental-mode standing-wave decay in rectangular tanks. He showed the decay decrement α_ν, due to viscous losses in an assumed oscillating laminar boundary layer on the tank walls and bottom, to be

$$\alpha_\nu \left(\frac{\pi}{\nu T k^2}\right)^{\frac{1}{2}} = \left(1 + \frac{\pi}{Bk}\right) - \frac{2kh}{\sinh 2kh} + \frac{\pi}{\sinh 2kh}. \tag{4}$$

Here, α_ν is defined as was α_T above, and B is tank width. The last term gives the contribution of the bottom boundary layer, the others the contributions of the wall layers.

Keulegan measured wave decay in smooth rectangular tanks of various sizes but similar shapes ($h/L = 0{\cdot}425$, $B/L = 0{\cdot}217$). For the largest tank used ($L = 242$ cm), the observed decay decrement α agreed closely with α_ν. For smaller tanks, α was significantly larger than α_ν. The discrepancy was attributed to surface tension. In hydrophilic basins (made of glass, and using distilled water and aqueous solutions, and alcohol), the difference between α and α_ν was found from a dimensional argument to be

$$\alpha_\gamma = K\frac{\gamma T^2}{\rho B^3}, \quad K = 0{\cdot}10. \tag{5}$$

(γ is surface tension.) In the hydrophobic basins (lucite, with distilled water), $K = 0{\cdot}6$. The data leading to this latter value are important to our work; they are shown in figure 7.

Miles (1967) wrote the total decay decrement as $\alpha_\nu + \alpha_L + \alpha_S$, where α_L represents wave decay due to capillary hysteresis, and α_S that due to the presence of a surface film. He gave expressions relating α_S and α_L to the degree and type of surface contamination, and the change of contact angle as the fluid moves up and down the tank walls. Unfortunately, we did not have the equipment necessary to measure these quantities, and cannot use these formulae in our data analysis. A rough calculation, based on reasonable estimates of the appropriate quantitites, suggests that $\alpha_\gamma \sim \alpha_L$. We shall use an argument similar to Keulegan's to find α_γ.

Case & Parkinson (1957) performed an experiment similar to that of Keulegan, using tap water of various depths in brass circular cylinders of radius 3·8 and 7·6 cm, and in a steel cylinder of radius 25·4 cm. They found α values of between two and three α_ν at first. Upon polishing the brass cylinders to a mirror finish, the differences between α and α_ν became very small. Some of the remaining discrepancy was attributed to surface tension; but the major portion was thought to be due to roughness elements on the tank bottom, which were well within the viscous boundary layer.

4. The experiment

We describe below a relatively simple experiment, designed to elicit information concerning the effect of convective turbulence on long waves.

4.1. *Apparatus*

The wave tank is shown in figure 1. The interior dimensions are 357·0 cm × 99·3 cm × 25 cm (length × width × height). The tank is much shallower and longer than those used by Keulegan, and by Case & Parkinson. The walls are half-inch Plexiglas, which is covered on the outside by one-inch styrofoam to minimize lateral heat transport. With tap water, the walls are hydrophobic. The bottom is a half-inch aluminum plate coated with teflon to avoid pitting. The plate can be heated to temperatures up to 65 °C, by passing current through a series of nichrome wires under it, spaced one inch apart and running the length of the tank. The heating rate is controlled by a rheostat. The bottom roughness

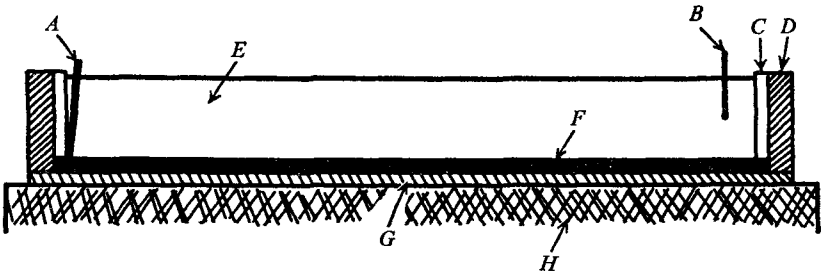

FIGURE 1. The bottom-heated wave tank. *A*, Wave maker. *B*, Capacitance wave gauge. *C*, Half-inch Plexiglas. *D*, Inch styrofoam. *E*, Water. *F*, Half-inch aluminum plate. *G*, Heating pad (nichrome wires in asbestos). *H*, Wood base.

was measured at $\frac{1}{2}$ mm intervals with a point micrometer having a precision of 10^{-4} cm: the r.m.s. bottom roughness height is $1{\cdot}25 \times 10^{-2}$ cm. The maximum height is about three times this value.

The difference in thermal expansion between the walls and bottom caused the walls to crack, and leaking to occur, in several earlier versions of the wave tank. The final solution was to fasten the above-mentioned thick Plexiglas walls to the aluminum bottom with machine screws, with a generous portion of silicone rubber sealer (RTV-106) between walls and bottom. Great care was taken to keep the inner corners of the tank free of excess rubber: an earlier, preliminary series of experiments had shown such extraneous roughness to lead to substantial deviations of α from α_v with the tank bottom at room temperature.

Waves are generated by a paddle wave maker at one end of the tank. Leaking around the paddle was eliminated by applying silicone rubber between the paddle and the tank walls and bottom. The waves are monitored with a capacitance wave gauge 5 cm from the other end of the tank, and recorded on a Leeds and Northrup Speedomax H strip-chart recorder. The gauge consists of a 36-gauge polythermaleze insulated wire with a transistorized detector, and is described fully by McGoldrick (1969). The gauge has a sensitivity of about 0·025 mm; it is strictly linear and practically free of drift; and it is insensitive to water-temperature variations. Calibrations before and after our experiments were the same; wetting of the dielectric coating of the wire was not a problem.

4.2. *Temperature structure*

Water temperatures at various points in the tank were found using thermocouples. Surface temperatures were measured with a radiation thermometer (Barnes PRT-5). At the maximum heating rate of the tank bottom, and a water depth of 21 cm, the Rayleigh number is 4×10^9. The time-mean vertical temperature profile (figure 2) is typical of buoyancy-driven turbulence, although it is slightly asymmetric with respect to mid-depth, owing to the difference in boundary conditions between the top and bottom water surfaces.

Typical temperature fluctuations at the surface, mid-depth, and a point 2 mm above the bottom, are also shown in figure 2. Both heat loss across the water surface and heat gain across the bottom are characterized by rapidly fluctuating

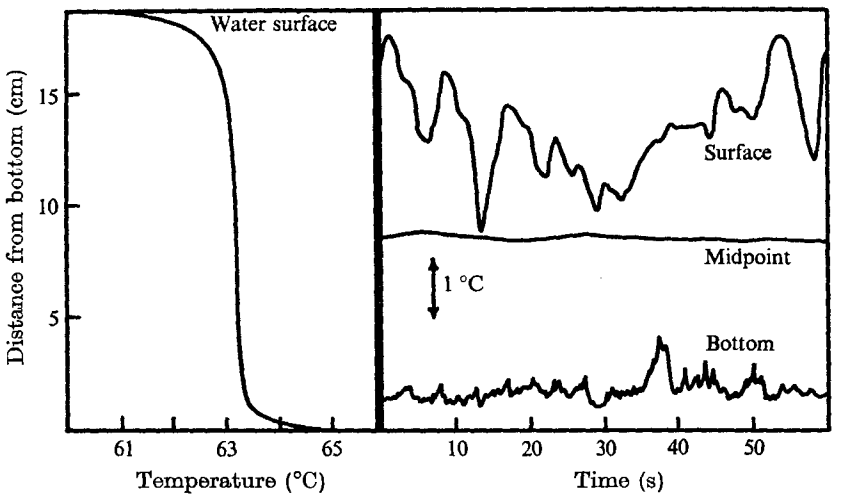

FIGURE 2. The mean temperature against distance from bottom (cm) of the heated wave tank, and temperature variations with time at the surface, mid-depth, and a point 2 mm above the bottom.

temperatures. Those at the surface are masked somewhat by the 0·3 s sampling time of the radiation thermometer. Only small fluctuations occur at mid-depth. These and other measurements are in general agreement with previous work on turbulent thermal convection, and mainly help to confirm that the water is in a steady convective state, and that any circulation caused by side-wall cooling is very weak.

4.3. *Velocity structure*

The general surface velocity structure was obtained from time-lapse photographs of small floating particles and powder. Horizontal vortices, of the order of centimetres in diameter, seem to be due to surface convergences concentrating the random surface vorticity that is generated by air sweeping in over the tank, replacing the air rising from near the water surface. Other air currents in the room were negligible. Although the vortices fluctuated in strength and moved slowly about, there was no evidence of circulation due to side-wall cooling. For $Ra \sim 4 \times 10^9$, the maximum observed fluid speed was about 4 cm s^{-1}, and the r.m.s. speed about 1 cm s^{-1}. These values compare favourably with the (vertical) speeds reported by Malkus (1954). Using this as an indicator of the kinetic energy in the water column, the wave and turbulent kinetic energies are comparable when the wave amplitude at the end of the tank is 1·5 mm.

There was no measurable surface-wave activity associated with the turbulent convection.

4.4. *Procedure*

The tank was filled with tap water, and allowed to reach a steady convective state. For large Ra, this took up to 12 h. Water was then drawn off to make h either 14, 16 or 18 cm. When the water temperature fluctuations again indicated a steady state, the wave maker was started, set at the fundamental resonant

frequency of the tank and at an angular amplitude of 0·73°. The waves attained their maximum amplitude in about half an hour. At this point, the wave maker was stopped in the vertical position, and the water-surface height measured until the waves were undetectable. This decay process took perhaps 10 min.

Water temperatures were taken at the surface, middepth, and bottom. The room temperature was constant to within at least 0·2 °C over an experiment. Tank-bottom temperature changes over an experiment were inconsequential.

5. Experimental results

An outline of the experiments conducted is given in table 1. Typical wave traces are shown in figure 3. The water surface was always glassy. The slight wave asymmetry at the larger wave heights can be reproduced using the second-order wave-maker theory of Milgram (1965) for cases close to resonance. Waves are monochromatic to the resolution of the wave gauge. Thus, wave scattering by the convective turbulence is unimportant, and the turbulent contribution to wave decay is associated with absorption.

5.1. *Measuring the total decay*

Wave heights were plotted against time on semilog paper (figure 4). The slope of the line then gave the total wave decay α. The line determined by the wave heights was very close to a straight line over a large number of wave periods. In the worst case, an uncertainty of $\pm 6 \times 10^{-4}$ was present in the slope measurement; the average uncertainty was $\pm 3 \times 10^{-4}$.

In each experiment, a distinct change in α was found somewhere in the wave-height range of 2·8–1·5 mm. This slope change is very likely associated with transition from a turbulent bottom boundary flow to a laminar flow. There is no general agreement on the point of transition from laminar to turbulent flow in an oscillating boundary layer. A summary is given by Kajiura (1968), according to whom the lowest transition Reynolds number $R = U_0\delta/\nu$ is 25 for a smooth bounding surface. U_0 is the maximum velocity just outside the boundary layer. Use of Lin's (1955) stability theory gives a much lower value (Collins 1963). The lowest reported transition Reynolds number for oscillating flow over a rough surface is $M = U_0 D/\nu = 15$ (Vincent 1957). D is the median diameter of grains of material on the bottom.

Our measured bottom roughness indicates that the tank bottom is in the transition range between smooth and rough surfaces. At room temperature, the Reynolds number M at the point of slope change was between 6 and 7·5. Here, the height of the largest roughness elements was used, as these are likely to control transition. This range in M shifted slowly upward with increasing Ra; at $Ra \sim 10^8$, $8 < M < 10$. It should be noted that our experiment involves a transition with decreasing Reynolds number; in the other studies mentioned above, transition occurred with increasing Reynolds number. Based on evidence dealing with other flows, it is not unreasonable to expect that boundary-layer turbulence in an oscillating flow, once present, will persist at Reynolds numbers less than the critical value.

Water depth (cm)	Bottom temperature (°C)	Surface temperature (°C)	*Ra* ($\times 10^{-8}$)	Measured decay decrement ($\times 10^{2}$)
14	19	19	0	2·697
				2·686
	28·5	30·6	1·4	2·436
				2·434
	40·9	43·6	3·1	2·230
				2·265
	47·1	50·6	4·9	2·204
				2·190
	55·3	59·5	7·5	2·200
				2·160
16	21·5	21·5	0	2·310
				2·321
	35·0	37·0	2·7	2·017
				2·032
	41·5	44·0	4·3	1·965
				1·927
	50·8	54·0	7·4	1·966
				1·946
	56·5	60·5	11·0	1·969
				1·971
18	19·5	19·5	0	2·102
	20·4	20·4		2·065
	24·0	24·0		2·000
	29·0	30·6	2·3	1·886
				1·892
	32·9	34·9	3·5	1·894
				1·865
	40·5	43·0	5·9	1·807
	47·0	50·0	8·8	1·839
	55·5	59·5	15·0	1·914
				1·914
				1·922

TABLE 1. Experimental results

The data analysis below deals only with wave decay after the distinct change in α. It is here that efforts to separate α_T from the other components of α were most successful. It is also here that the simple model given above most likely applies, and that Keulegan's theory is valid.

5.2. *Interpretation of the data*

Our goal is to estimate the contribution of convective turbulence to the observed long-wave decay. Unfortunately, the relatively inefficient heat transfer across the air–water interface and the small size of the room meant that the average

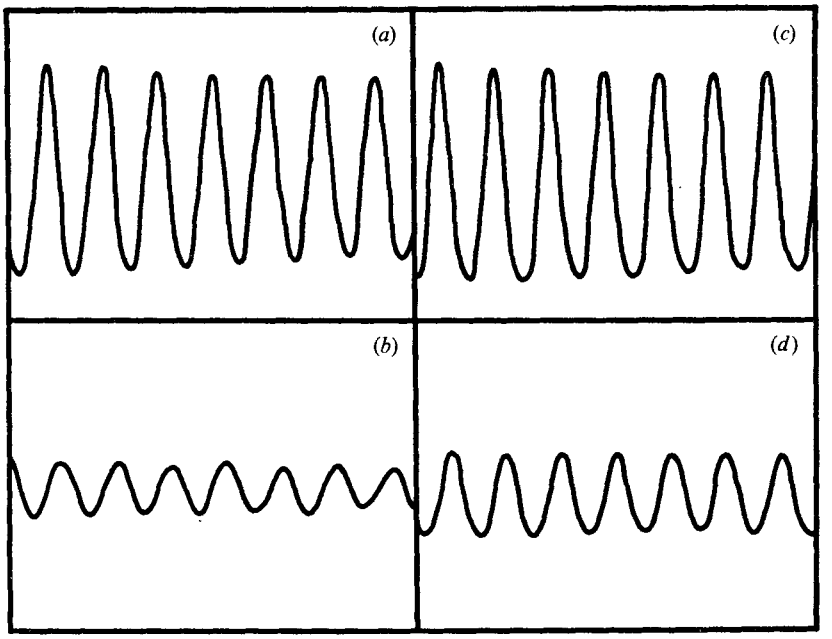

FIGURE 3. Typical wave traces after the wave maker was stopped: (*a*) and (*b*) are at room temperature; (*c*) and (*d*) are at a mean water temperature of 57·5 °C, and $Ra = 1{\cdot}5 \times 10^9$.

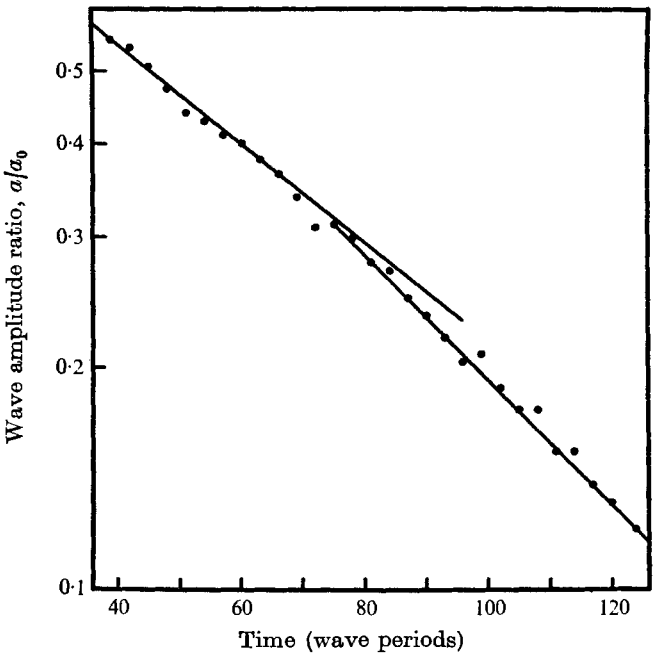

FIGURE 4. Wave amplitude ratio a/a_0 against time (wave periods), showing the slope change associated with boundary-layer transition. For clarity, only part of the data are shown; the best-fit lines are based on more data, over a larger number of wave periods. $h = 18$ cm, $Ra = 1{\cdot}5 \times 10^9$, $\alpha = 1{\cdot}922 \times 10^{-2}$.

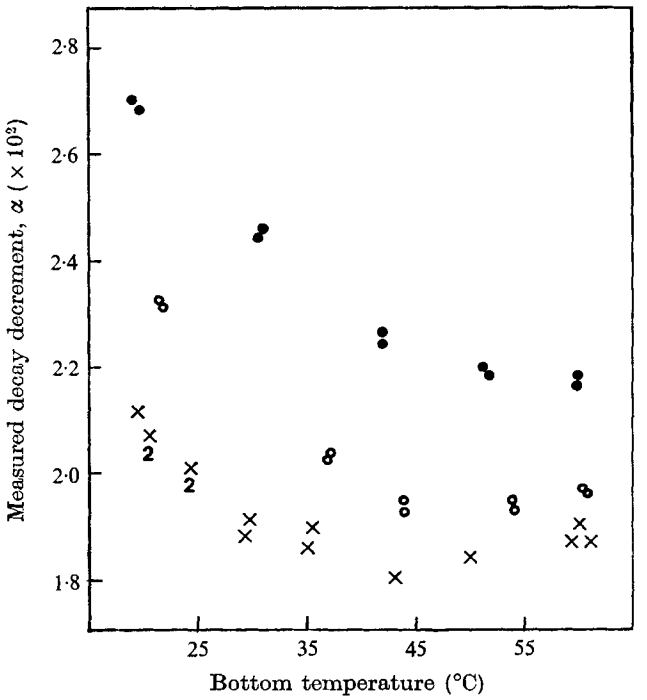

FIGURE 5. The measured logarithmic wave-decay decrement α against tank bottom temperature (°C): ●, h = 14 cm; ○, 16 cm; ×, 18 cm.

water temperature $\langle T \rangle$ had to be raised substantially to achieve the vertical density gradients necessary for significant turbulence. This resulted in large relative changes in ν, and perhaps also in surface-film and contact-angle characteristics.

It is quite clear that the turbulence acts to increase wave decay with increasing Ra. Figure 5 shows the measured total decay rates against mean water temperature. Bearing in mind that Ra increases with $\langle T \rangle$, that ν decreases with increasing temperature, and that the major contributor to α is viscous decay, there is little doubt that α first decreases with increasing $\langle T \rangle$ because the viscous term α_ν diminishes, and that α later increases with $\langle T \rangle$ because of the increased influence of α_T.

There have been few measurements of the effect of temperature on moving contact angles, so that it is impossible to ascertain α_L. Because of this and similar problems related to α_S, we resort to Keulegan's procedure and write

$$\alpha = \alpha_\nu + \alpha_\gamma + \alpha_T.$$

Then, to estimate α_T we must estimate α_ν and α_γ. In particular, we must allow for the effects of increasing temperature on these quantities, which will necessitate some reasonable but perhaps debatable assumptions. Because of this, we shall review the data interpretation in some detail, and we shall obtain upper and lower bounds for α_T as a function of Ra.

(i) *The viscous decay decrement.* The decay decrement, due to boundary-layer

viscosity in a smooth rectangular container, is given by (4). We shall use a modified version of (4) to estimate the viscous decay in the heated tank. That this is appropriate must be regarded as an assumption. However, it is consistent with others made in the course of the work, and there seems to be little hope of any further analysis of the data without making this step. We attempt to evaluate its validity below.

Keulegan's derivation of (4) involves integrating terms such as $(\partial u/\partial z)^2$ over the volume of the bottom boundary layer, and over a wave period. Here, the velocity component along the tank u is chosen as a reasonable local correction to the inviscid interior flow, such that the bottom no-slip condition is met. Equation (4) is rather insensitive to the precise form of u, due to the integrations.

In keeping with the spirit of our analysis, we assume that the x component of velocity in the boundary layer can be written as the sum of the wave-induced component u_w and the contribution due to convection u_c. Since the space scales governing u_w and u_c are quite different, and since the convective activity should be periodic in the cross-tank direction,

$$\overline{\left(\frac{\partial u}{\partial z}\right)^2} \sim \overline{\left(\frac{\partial u_w}{\partial z}\right)^2} + \overline{\left(\frac{\partial u_c}{\partial z}\right)^2}.$$

That is, the viscous energetics are likely to be independent.

A more difficult question to resolve is whether the convective activity has a marked effect on u_w. Such an effect would probably enter through a nonlinear term in the momentum equation, such as $u\,\partial u/\partial x$. Since $\partial u_w/\partial t$ must be a large term in the oscillatory boundary layers, and since u_c and u_w are probably uncorrelated in the cross-tank direction, the r.m.s. ratio of this term to the convective component of the cross-tank average of $u\,\partial u/\partial x$ is indicative of the interaction. Because very little is known about the high-Ra conductive boundary layer, we must resort to a scale analysis to determine the ratio.

The conductive length scale is L_c. An estimate for the velocity scale U_c is obtained from boundary-layer mass conservation and the (limited) information available regarding the vertical velocity in thermals:

$$U_c = nWL_c/(2\Delta).$$

Here L_c has been identified with a mean radius about one active site of thermal generation. Then the ratio of terms is

$$\Lambda = \left(u_c \frac{\partial u_c}{\partial x}\right)_{\text{r.m.s.}} \left(\frac{\partial u_w}{\partial t}\right)^{-1}_{\text{r.m.s.}} \sim n^2 W^2 L_c \left[8\Delta^2 \left(\frac{\partial u_w}{\partial t}\right)_{\text{r.m.s.}}\right]^{-1}.$$

On the basis of the small amount of experimental information available, we choose the c.g.s. values $L_c \sim 0{\cdot}5$ and $nW \sim 0{\cdot}02$. These, together with calculated values of Δ and $(\partial u_w/\partial t)_{\text{r.m.s.}}$, give $\Lambda \sim 0{\cdot}02$. Thus, the interactive terms in the equations describing the oscillatory boundary layer seem unimportant.

This argument is not altogether convincing; the scale estimates are only plausible. However, it is at least not unreasonable to assume that the integral characteristics of the oscillatory boundary layer are not significantly affected by the presence of the convective activity, and that (4) can be used to sort out the viscous contribution to wave decay.

Water depth (cm)	Bottom temperature (°C)	Conduction boundary layer thickness $\Delta = 3(\rho c T\kappa^3/gQ)^{\frac{1}{4}}$ (mm)	Oscillating boundary layer thickness $\delta = (\nu/\sigma)^{\frac{1}{2}}$ (mm)
14	30·6	0·56	0·88
	43·6	0·51	0·78
	59·5	0·44	0·69
16	37·0	0·57	0·80
	54·0	0·48	0·70
	60·5	0·45	0·66
18	34·9	0·57	0·80
	50·0	0·50	0·70
	59·5	0·45	0·65

TABLE 2. Typical boundary-layer thicknesses

The teflon treatment left the tank bottom slightly roughened. This resulted in a small increase in the total area encountered by the water in the bottom boundary layer. For the small water velocities associated with the standing-wave heights below that at which the above-mentioned change in α occurs, it seems most reasonable to assume that the bottom boundary-layer flow follows the bottom contour. A similar assumption was used by Benjamin (1959) to study steady shearing flow over a small-amplitude wavy wall. It should be noted that the boundary-layer thicknesses Δ and δ were both an order of magnitude greater than the r.m.s. bottom roughness (table 2).

Our situation is sufficiently unlike that of Benjamin, and our bottom-roughness data so limited by available instrumentation, that it is impossible to use his work to calculate the bottom shear stress. We note, however, that Benjamin found a slight, but periodic, deviation from the stress obtained simply by taking the boundary-layer flow associated with a flat bottom to be bent, to follow the curved bottom. Such periodic variation would not affect the total momentum transfer from the water.

We shall express both the area increase over that of a smooth, flat bottom and any possible net increase in stress (associated, say, with a higher-order treatment along the lines of Benjamin's work) in terms of an effective bottom area $L'B'$. Two estimates of $L'B'$ are made, which give reasonable bounds on the total contribution of bottom stress to wave decay. The bounds given by the resulting estimates of α_T will be one measure of the uncertainty of the results.

When the effective bottom area is used to derive the viscous contribution to the total decay decrement, while the actual length L is retained for calculating the resonant frequency, we obtain the effective viscous decay decrement

$$\alpha_{ve} = (\nu_m T/\pi)^{\frac{1}{2}}\left\{\frac{\pi}{B} + k - \frac{2k^2h}{\sinh 2kh}\right\} + (\nu_b T/\pi)^{\frac{1}{2}}\frac{k^2L'B'}{B\sinh 2kh}. \tag{6}$$

ν_m, ν_b are the mid-depth and bottom viscosities.

Water depth (cm)	α ($\times 10^2$)	α_{ve} ($\times 10^2$)
14	2·697	2 052
	2·686	2·052
16	2·310	1·735
	2·321	1·735
18	2·102	1·577
	2·065	1·560
	2·000	1·496

TABLE 3. Theoretical viscous and measured decay decrements at room temperature. The theoretical viscous decrement is based on an assumed sinusoidal bottom, as discussed in the text.

(ii) *A lower bound on* α_T. The effective bottom area can be estimated from our bottom-roughness data in several ways. Simply connecting the measured points with straight lines gives a lower bound for the total encountered length of the tank. A more realistic lower estimate is obtained by connecting each adjacent pair of measured points with a half sine wave, with crest and trough at the points. This procedure gives $L' = 375{\cdot}75$ cm. A similar approach gives the encountered bottom width, $B' = 104{\cdot}51$ cm. Although other, more sophisticated models could be used, none is free from objection. Any increase in effective area, due to an increase in shear stress, has been neglected.

The measured decay decrements at room temperature are compared with α_{ve} in table 3. The theoretical values are about 25 % lower than the observed. The discrepancy may be due to form drag associated with large, isolated bottom roughness elements, or with irregularities in the RTV sealer between tank walls and bottom. It may also be due to capillary hysteresis and surface films.

The tank walls are very smooth; almost all the RTV is along the bottom seams or the edges of the wave-maker paddle. The oscillatory bottom boundary layer δ is thicker at smaller depths. If form drag were the major cause for the difference between α and α_{ve} at room temperature, this difference should either decrease or remain constant with decreasing water depth. This is not the case: the difference increases with decreasing depth.

The importance of surface activity can be examined by plotting $\alpha - \alpha_{ve}$ against $\gamma T^2/(\rho B^3)$ (figure 6). The plot is quite linear, and passes through the origin without undue forcing. That is, we find, as did Keulegan, that the discrepancy can be expressed as

$$\alpha - \alpha_{ve} = K\gamma T^2/(\rho B^3). \tag{7}$$

However, we find $K = 1{\cdot}89$, compared with Keulegan's value $K = 0{\cdot}6$. For comparison, we have plotted both our room-temperature values of $\alpha - \alpha_{ve}$ and those of Keulegan in figure 7. Since the dimension ratio B/L of our channel is quite close to that of the Keulegan channels, this comparison is meaningful. Our data are a logical extrapolation of his lower values. Keulegan observed that the total wave decay α increases with decreasing wave amplitude. Since the

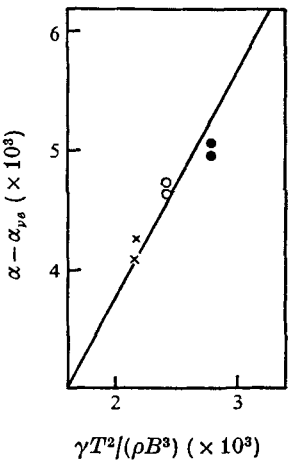

FIGURE 6. The discrepancy between the measured decay decrement α and the effective viscous decay decrement $\alpha_{\nu s}$ (based on a sinusoidal fit to the measured bottom variations) at room temperature against Keulegan's (1959) surface-tension parameter $\gamma T^2/(\rho B^3)$. The straight line shown also passes through the origin.

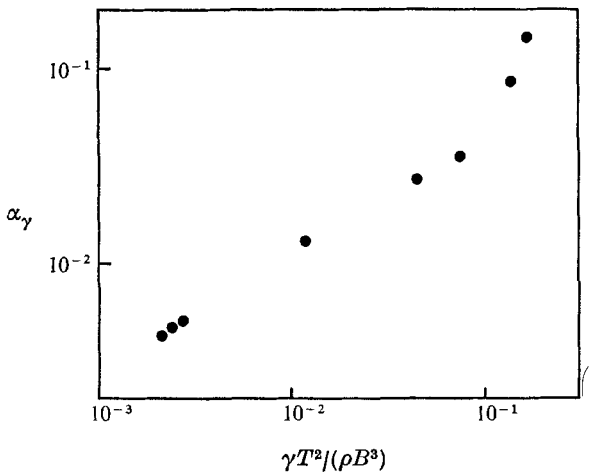

FIGURE 7. The discrepancy between the measured and effective viscous decay decrements: $\alpha_\gamma = \alpha - \alpha_{\nu s}$ against $\gamma T^2/(\rho B^3)$. The three points for small $\gamma T^2/(\rho B^3)$ denote average values of our data for each of the three water depths at room temperature; the other five points are plotted from Keulegan's (1959) calculations of $\alpha - \alpha_\nu$.

surface-activity contribution is independent of amplitude, it is quite possible that the decay in his smaller basins was not observed sufficiently long for the increase in α to occur. Thus, the agreement of the K values may be expected to improve when one compares the results from only the larger channels.

We now use our estimate of K to determine α_γ at higher temperatures. Since γ was found to decrease only slightly with increasing water temperature, the estimated values of α_γ at higher temperatures are quite close to those at room temperature; little if any extrapolation is necessary.

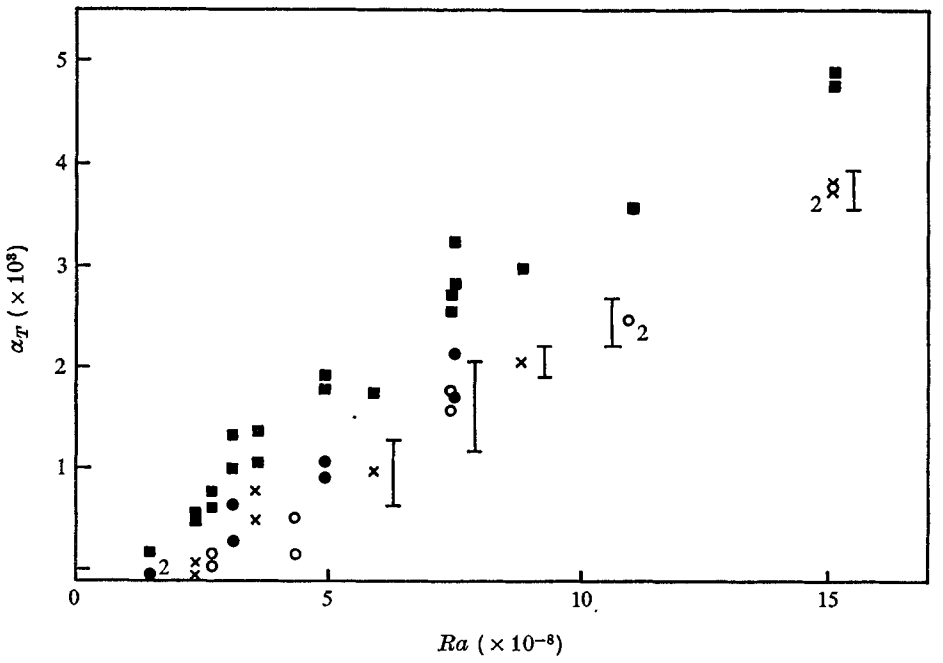

FIGURE 8. The turbulent decay decrement $\alpha_T = \alpha - \alpha_\gamma - \alpha_{ve}$ against Rayleigh number, based on a sinusoidal fit to the measured bottom variations: ●, h = 14 cm; ○, 16; ×, 18. A 2 denotes two independent measurements which coincide. A ■ denotes an upper bound on α_T, calculated as outlined in the text.

The values of α_T obtained from $\alpha_T = \alpha - \alpha_{ve} - \alpha_\gamma$ and (6) and (7) are plotted against Rayleigh number in figure 8. Despite a good amount of scatter for small Ra, the data for different water depths are quite consistent for larger Ra, and increase linearly with increasing Ra. The error bounds shown are based on the uncertainty in determining α from the experimental data. In the interest of clarity, they are plotted only for certain, higher α_T values found using the two greater depths. These are typical values, although the ambiguity in α decreased somewhat at greater Ra, and with increasing water depth.

(iii) *An upper bound on* α_T. Since the surface-tension contribution to the decay decrement changes little with increasing water temperature, while the viscous contribution decreases markedly, we can obtain an upper bound on α_T by assuming α_γ to be negligible at room temperature. We find that the effective area ratios $L'B'/LB$, such that the entire decay at room temperature is due to viscosity, are 1·43 (h = 14 cm), 1·47 (16 cm), and 1·48 (18 cm). These values are quite consistent; the slight increase at greater depths could be due to a small corresponding decrease in δ. Using the average effective area to estimate α_{ve} at higher temperatures, and thus α_T from $\alpha - \alpha_{ve}$, gives the upper bounds on α_T shown in figure 8.

6. Discussion

On the basis of the data shown above, we propose the relation

$$\alpha_T \sim 2{\cdot}5 \times 10^{-12} Ra, \quad Ra < 2 \times 10^9.$$

This relation is based on a number of interpretive assumptions, and is perhaps best viewed as a lower bound. However, the agreement of the data at different depths when scaled against Ra, and of α_γ with Keulegan's data, lend one confidence in the formula.

Calculations similar to those above, but based on the straight-line approximations to L' (360·70 cm) and B' (100·32 cm), show slightly better agreement of α_γ with Keulegan's data, and give α_T values 5–10 % lower than those obtained using the sinusoidal approximation. However, several α_T for smaller Ra are then less than zero, which suggests that this interpretation gives an unnecessarily severe lower bound on α_T. None the less, the calculation does show that α_T is rather insensitive to variations of the effective area. This is reassuring, as $L'B'$ is chosen somewhat arbitrarily.

The simple model for α_T, described at the outset, depends on superposing convective thermals on the wave-induced oscillating shear flow. That this reflects the actual situation is an assumption, and open to question. Dimensional reasoning implies that $\alpha_T = F(Ra, Ri, Pr)$, where Pr is the Prandtl number, and Ri a suitable Richardson number. If an interaction between the conduction and oscillatory boundary layers is important, a boundary-layer Richardson number should also be important. On the other hand, good correlation of α_T with Ra suggests that boundary-layer interactions are less important than the integral properties of the flow, which is implied in our treatment of τ as a body force.

We define the Richardson number as

$$Ri = \beta g \delta^2 (T_m - T_b)/(U_s^2 \Delta).$$

U_s is the long-wave velocity amplitude at the $a(t)$ slope change discussed above. To calculate the upward heat flux Q (and so Δ), we use the relation between Nusselt and Rayleigh numbers due to Rossby (1969)

$$Nu = 0{\cdot}131 Ra^{0{\cdot}30}.$$

This describes heat transfer at high Ra in a fluid between two rigid boundaries. Figure 9 shows α_T plotted against Ri. The results at different water depths do not scale well. A similar result is obtained when α_T is plotted against Pr; and it is apparent that Ra is the dominant parameter governing the measured long-wave decay due to convective turbulence.

The relation of δ to Δ is of some interest, and typical values are shown in table 2. The ratio δ/Δ is always close to 1·5, although it increases slightly both with increasing temperature and with decreasing depth. This slight variation implies that the flow regime remains substantially the same over our range of experimental conditions. Because of the small change of Δ with water depth, a local Rayleigh number based on Δ is not useful in reducing the experimental data to a single curve.

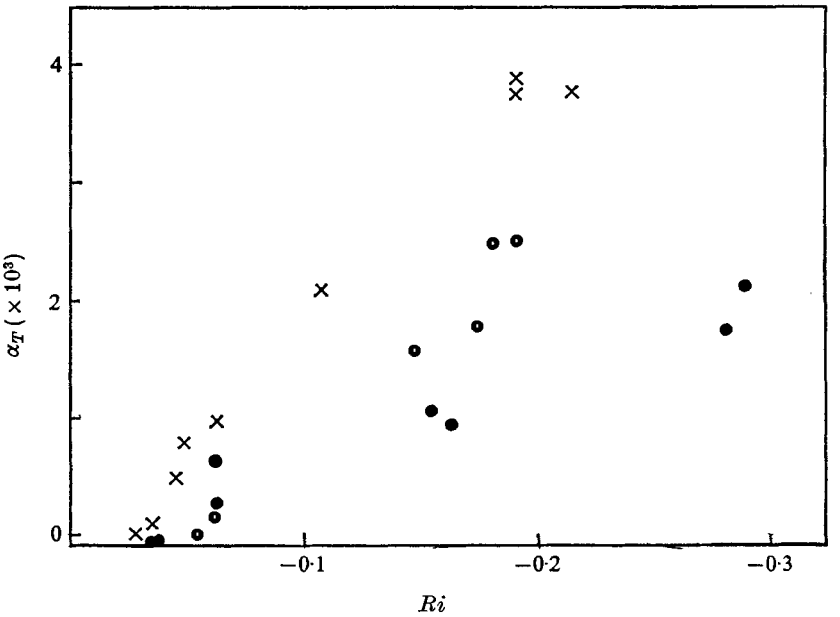

FIGURE 9. The turbulent decay decrement α_T against a boundary-layer Richardson number Ri defined in the text: ●, h = 14 cm; ○, 16; ×, 18.

Finally it is interesting to compare the experimental results with the simple theory given at the outset, (3), when other, independent data are used to evaluate n and W. The measurements and pictures of Sparrow *et al.* (1970) suggest that $n = O(10^{-2})$ for our higher bottom temperatures. The velocity measurements of Malkus suggest $W \sim 2{\cdot}5\,\mathrm{cm\,s^{-1}}$ for $Ra = 1{\cdot}5 \times 10^9$. These give $\alpha_T \sim 4 \times 10^{-3}$, which is the same order of magnitude as our experimental value. Although this agreement rests uneasily upon the estimate of n, both it and the scaling of α_T with Ra do lend credence to the assumption that the convective turbulence (including the conduction layer), and the oscillatory boundary layer do not interact to a significant degree in the experimental range in which we worked.

The wave tank was designed and constructed by Mr J. C. Buchholtz. Some preliminary experimental work was done by Mr D. H. Kim. We also benefited from several discussions with Professor E. N. Lightfoot. This work was supported by the University of Wisconsin Sea Grant Program, under the National Oceanic and Atmospheric Administration's Office of Sea Grant, U.S. Department of Commerce.

REFERENCES

BENJAMIN, T. B. 1959 Shearing flow over a wavy boundary. *J. Fluid Mech.* **6**, 161.

CASE, K. M. & PARKINSON, W. C. 1957 Damping of surface waves in an incompressible liquid. *J. Fluid Mech.* **2**, 172.

COLLINS, J. I. 1963 Inception of turbulence at the bed under periodic gravity waves. *J. Geophys. Res.* **68**, 6007.

DEARDORFF, J. W. & WILLIS, G. E. 1967 Investigation of turbulent thermal convection between horizontal plates. *J. Fluid Mech.* **28**, 675.

GREEN, T., MEDWIN, H. & PAQUIN, J. E. 1972 Measurements of surface wave decay due to underwater turbulence. *Nature*, **237**, 115.

HOWARD, L. N. 1966 Convection at high Rayleigh number. *Proc. 11th Cong. Appl. Mech.* (ed. H. Görtler). Springer.

KAJIURA, K. 1968 A model of the bottom boundary layer in water waves. *Bull Earthquake Res. Inst.* **46**, 75.

KEULEGAN, G. H. 1959 Energy dissipation in standing waves in rectangular basins. *J. Fluid Mech.* **6**, 33.

LIN, C. C. 1955 *The Theory of Hydrodynamic Stability*. Cambridge University Press.

MCGOLDRICK, L. F. 1969 A system for the generation and measurement of capillary-gravity waves. *Department of Geophysical Science University of Chicago, Tech. Rep.* 3.

MALKUS, W. V. R. 1954 Discrete transitions in turbulent convection. *Proc. Roy. Soc.* A **225**, 185.

MILES, J. W. 1967 Surface wave damping in closed basins. *Proc. Roy. Soc.* A **297**, 459.

MILGRAM, J. H. 1965 Compliant water-wave absorbers. *Massachusetts Institute of Technology, Department of Naval Architecture and Marine Engineering, Rep.* 65–13.

PHILLIPS, O. M. 1959 The scattering of gravity waves by turbulence. *J. Fluid Mech.* **5**, 1177.

ROSSBY, H. T. 1969 A study of Bénard convection with and without rotation. *J. Fluid Mech.* **36**, 309.

SPARROW, E. M., HUSAR, R. B. & GOLDSTEIN, R. M. 1970 Observations and other characteristics of thermals. *J. Fluid Mech.* **41**, 793.

TOWNSEND, A. A. 1959 Temperature fluctuations over a heated horizontal surface. *J. Fluid Mech.* **5**, 209.

VINCENT, G. E. 1957 Contribution to the study of sediment transport on a horizontal bed due to wave action. *Proc. 6th Conf. Coastal Engineering*, Florida, p. 326.